

High-resolution structure studies and magnetoelectric coupling of relaxor multiferroic $\text{Pb}(\text{Fe}_{0.5}\text{Nb}_{0.5})\text{O}_3$

Hasung Sim,^{1,2,*} Darren C. Peets,^{1,2} Sanghyun Lee,^{1,3} Seongsu Lee,⁴ T. Kamiyama,³ K. Ideda,³ T. Otomo,³ S.-W. Cheong,⁵ and Je-Geun Park^{1,2,†}

¹*Center for Correlated Electron Systems, Institute for Basic Science (IBS), Seoul 151-747, Korea*

²*Department of Physics and Astronomy, Seoul National University, Seoul 151-747, Korea*

³*Institute of Materials Structure Science and J-PARC Center, KEK, Tsukuba 305-0801, Japan*

⁴*Neutron Science Division, Korea Atomic Energy Research Institute, Daejeon 305-353, Korea*

⁵*Rutgers Center for Emergent Materials and Department of Physics and Astronomy, Rutgers University, Piscataway, New Jersey 08854, USA*

$\text{Pb}(\text{Fe}_{0.5}\text{Nb}_{0.5})\text{O}_3$ (PFN), one of the few relaxor multiferroic systems, has a G -type antiferromagnetic transition at $T_N = 143$ K and a ferroelectric transition at $T_C = 385$ K. By using high-resolution neutron-diffraction experiments and a total scattering technique, we paint a comprehensive picture of the long- and short-range structures of PFN: (i) a clear sign of short-range structural correlation above T_C , (ii) no sign of the negative thermal expansion behavior reported in a previous study, and (iii) clearest evidence thus far of magnetoelectric coupling below T_N . We conclude that at the heart of the unusual relaxor multiferroic behavior lies the disorder between Fe^{3+} and Nb^{5+} atoms. We argue that this disorder gives rise to short-range structural correlations arising from O disorder in addition to Pb displacement.

PACS numbers: 75.85.+t, 61.05.F-, 75.40.-s

INTRODUCTION

It is rare in nature to find a single system which hosts two or more ordered ground states out of otherwise unconnected degrees of freedom. If multiple ordered ground states exist, a natural question to ask is whether they are connected to one another. Although the same electrons may be responsible for multiple degrees of freedom, allowing coupling of the various forms of order, this is uncommon, making materials in which they are coupled particularly interesting. Magnetoelectric multiferroic materials, in which ferroelectricity and magnetism coexist and are coupled, are an example of just such a material. The ability to control one form of order via another offers a huge potential for technological applications and, at the same time, poses new challenges for our understanding of how distinct degrees of freedom as disparate as bulk polarization and magnetization can be coupled to one another [1, 2]. Here the sought-after coupling, so-called magnetoelectric effects, can lead to better manipulation of unusual multiferroic behavior and to exotic excitations of mixed character. Despite the huge interest, however, the origin of magnetoelectric coupling has often proven challenging to address experimentally for a given material.

Lead iron niobate $\text{Pb}(\text{Fe}_{0.5}\text{Nb}_{0.5})\text{O}_3$ (PFN) is a multiferroic material with a ferroelectric transition at $T_C = 385$ K [3] and an antiferromagnetic transition at $T_N = 143$ K [3–6] which is known to be G -type [7]. It is noteworthy for its high dielectric constant, which changes at both the ferroelectric [4, 8, 9] and the magnetic transitions [3, 9, 10] and is strongly frequency dependent. Its reported high dielectric constant makes it a suitable can-

didate material for multilayer ceramic capacitors among other electronic devices. The reported strong frequency dependence, making it a rare example of a relaxor multiferroic, most likely arises from disorder at the magnetic B site of the perovskite structure. Since many ferroelectric systems have disordered magnetic ions on the B site, a full understanding of PFN might well have wider implications for finding or optimizing other relaxor multiferroic materials for potential applications.

Despite the interest in the physical properties of PFN, however, several features of the underlying crystal structure still remain unresolved. For example, two competing space groups, $R3m$ [7] and Cm [11, 12], have been proposed for the low-temperature structure, and there is an unconfirmed report of negative thermal expansion below the antiferromagnetic transition [11]. In attempting to characterize the relaxor behavior, several groups have investigated the local structure [13, 14], which is closely associated with relaxor behavior in ferroelectrics, and discussed the possibility of structural disorder both experimentally [14, 15] and theoretically [16]. These studies notwithstanding, the key questions, we believe, are yet to be fully answered. For instance, it will be interesting to know how the relaxor behavior is connected to the short-range local structure. More importantly, one first has to know the exact details of the local distortion and, if possible, the structural basis of the sought-after magnetoelectric coupling.

In order to address these questions, we have undertaken full high-resolution neutron powder-diffraction studies as well as total scattering experiments using two state-of-the-art instruments: S-HRPD and NOVA, both at J-PARC, in Tokai, Japan. For this kind of study it is

essential to be able to examine both long- and short-range structures simultaneously as performed for other ferroelectric materials [17]. By combining data obtained from both instruments, we conclude that the low-temperature space group is Cm with clear signs of the short-range structure surviving even above the ferroelectric transition temperature, offering an explanation for the relaxor behavior. Neither experiment showed signs of negative thermal expansion. We then uncovered structural signatures of the magnetoelectric coupling by analyzing the temperature dependence of the electric polarization calculated from the structure parameters. Our detailed analysis of the local structure leads us to the conclusion that both Pb displacement and O disorder are exhibited in this material.

EXPERIMENTAL DETAILS

About 7 g of polycrystalline PFN samples were prepared by a standard solid-state method. Stoichiometric PbO , Fe_2O_3 , and Nb_2O_5 were mixed, then calcined in air at 850°C for 2 days. After calcination the products were ground, pressed into pellets, and then sintered at 1050°C for 1 day. The samples were verified to be single phase with a Rigaku Miniflex II x-ray diffractometer as well as the later high-resolution neutron diffraction studies which form the main body of this paper.

High-resolution neutron time-of-flight powder-diffraction experiments were carried out using the S-HRPD beamline at J-PARC, Tokai, Japan, on a powder sample in a cylindrical vanadium can, at ten temperatures from 10 to 300 K. Rietveld refinement of the diffraction data was performed using FULLPROF [18]. The subsequent total scattering experiments were carried out using a vanadium-nickel sample can at the NOVA beamline at J-PARC with a maximum Q value of $Q_{max} = 30 \text{ \AA}^{-1}$ at five temperatures between 62 and 453 K. Sample environment constraints prevented measurements above the ferroelectric transition temperature at S-HRPD, so NOVA was also used to collect diffraction patterns at selected higher temperatures. For the local structure study, a radial distribution function was calculated from the total scattering data and analyzed using PDFGUI [19]. The experimentally obtained $S(Q)$ was then Fourier transformed into real space to obtain the atomic pair distribution function $G(r)$ as follows:

$$G(r) = 4\pi r [\rho(r) - \rho_0] = \frac{2}{\pi} \int_0^{Q_{max}} [S(Q) - 1] \sin Qr dQ,$$

where $\rho(r)$ and ρ_0 are the atomic number density and the average number density, respectively, and Q_{max} is the maximum scattering wave vector. $G(r)$ was modeled using $4 \times 4 \times 4$ supercells for several different models of the short-range structure.

RESULTS AND DISCUSSION

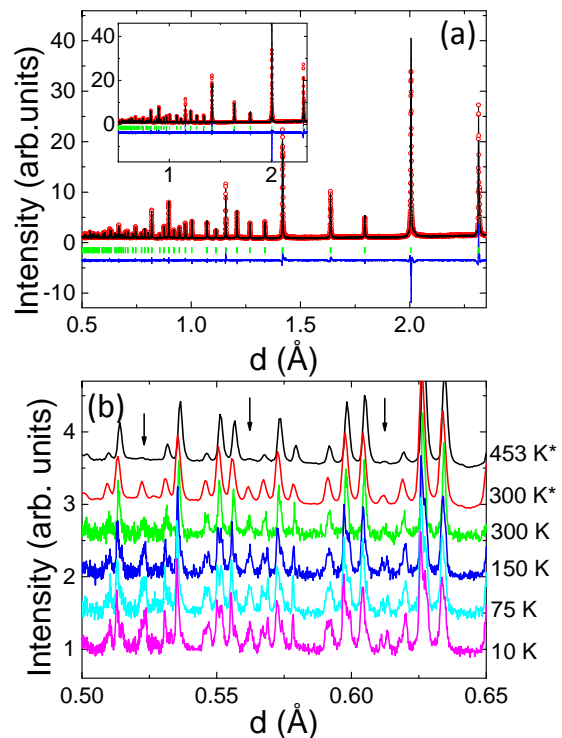


FIG. 1. (a) Neutron powder-diffraction patterns with refined results in the Cm and $R3m$ (inset) space groups, respectively, at 300 K. Circles represent data, a line the refinement, and the line at the bottom the residual, whereas green vertical bars mark the Bragg positions. (b) Diffraction patterns at several temperatures. The upper two datasets (starred) are NOVA results, and the others are S-HRPD results. Several peaks disappear above $T_C = 385$ K due to the structural transition (arrows).

The low-temperature space group of PFN is thought to be the monoclinic space group Cm , but as discussed, the $R3m$ space group has also been proposed as an alternative structure; to the best of our knowledge it is still not settled which one of the two space groups is correct. Figure 1(a) shows the neutron powder-diffraction pattern and its refinement results in the Cm and $R3m$ (inset) space groups at 300 K. We assumed that Fe and Nb are randomly distributed at the same crystallographic position [7, 11, 12] and allowed this sublattice to shift relative to Pb but did not split any sites at this stage. Satisfactory refinements have previously been reported in both $R3m$ [7] and Cm [11]; we rely on an additional approach to distinguish these space groups. The data are well explained by both structures, although the quality of the refinement is slightly better in Cm , but this is not surprising since the Cm structure model has more free parameters. Table I summarizes the refined structural parameters for the 300 K data in the Cm and $R3m$ structures. Results are described in the rhombohedral setting

of the $R3m$ structure for comparison with Ref. 7. One can also convert the lattice parameters of the Cm structure to pseudocubic notation to ease comparison with the paraelectric structure as performed in Fig. 3(a) [20].

TABLE I. Refined structure parameters at 300 K in the Cm (with b as the unique monoclinic axis and cell choice 2) and $R3m$ structures. The unsplit Pb position is taken as the origin in Cm , whereas the Fe/Nb position is set to (0.5,0.5,0.5) for $R3m$ to aid comparisons to the literature.

Cm	$a_m = 5.6819(1) \text{ \AA}, b_m = 5.6738(1) \text{ \AA}, c_m = 4.01202(5) \text{ \AA}, \beta = 89.896(2)^\circ$			
Ions	x	y	z	$B (\text{\AA}^2)$
Pb	0.0000	0.0000	0.0000	1.82(8)
Fe/Nb	0.4669(9)	0.0000	0.5165(18)	0.34(3)
O1	0.4333(13)	0.0000	0.0002(26)	0.54(3)
O2	0.2129(20)	0.2483(7)	0.4989(29)	0.54(3)
$R_p: 5.26, R_{wp}: 7.68, R_{exp}: 4.13, \chi^2: 3.45$				
$R3m$	$a_r = 4.01389(3) \text{ \AA}, \alpha = \beta = \gamma = 89.9223(2)^\circ$			
Pb	0.0205(6)	0.0205(6)	0.0205(6)	2.45(5)
Fe/Nb	0.5000	0.5000	0.500	0.27(2)
O	0.4772(2)	0.4772(2)	-0.0092(5)	0.58(2)
$R_p: 5.48, R_{wp}: 8.01, R_{exp}: 4.13, \chi^2: 3.76$				

In the temperature-dependent data, magnetic peaks can be observed at $d = 1.55$ and 1.85 \AA , consistent with the reported G -type antiferromagnetic structure [7]. Several structural peaks, shown in Fig. 1(b), are absent above the ferroelectric transition of 385 K as seen comparing the data taken at 453 and 300 K; these peaks are marked by arrows. We note that we can refine the highest temperature data in the paraelectric phase using the previously reported space group $Pm\bar{3}m$ [12, 15, 21]; however, as we will discuss later, there are clear signs of short-range structure in the total scattering data even at 453 K.

In order to distinguish the two candidate low-temperature space groups, the temperature dependence of the peak widths for several nuclear Bragg peaks as obtained from fits to a Lorentzian line shape was examined, and a search was performed for peaks that are split in one space group but not the other. The large number of reflections in this low-symmetry structure makes it difficult to find nonoverlapping peaks, but several good candidates were located. The (002) and (220) Bragg reflections of the Cm structure, shown in the inset of Fig. 2(a), were found to be the most suitable: In the $R3m$ space group the resulting peak contains only one unique reflection, (200). No clear splitting is observed at low temperatures, but the peak width increases markedly on cooling as shown in Fig. 2(a), which is exactly opposite to what one expects from any conventional thermally

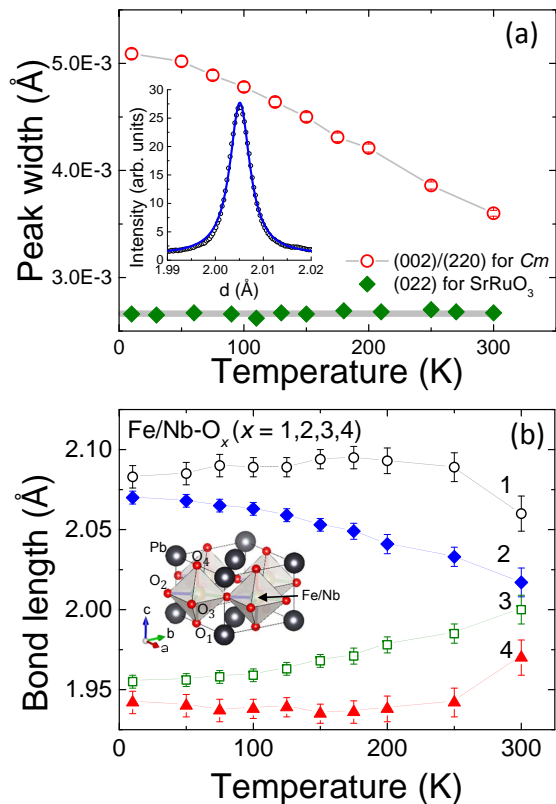


FIG. 2. (a) Temperature dependence of the peak width of the (002)/(220) Bragg peak in the Cm structure with the raw data at 10 K shown in the inset. Error bars are smaller than the symbol size. The data for the (022) peak of $SrRuO_3$ were taken after Ref. [22] (see the text). (b) Temperature dependence of Fe/Nb-O bond lengths. The inset depicts the structure of PFN with the Cm space group: There are four different Fe/Nb-O bonds denoted by the numbers.

activated broadening process. Similar temperature dependence is observed in other peaks, which are split in Cm and not in $R3m$. As we cannot find a peak from a well-separated Bragg reflection in our data because of the low symmetry, we choose $SrRuO_3$ measured under almost identical conditions in order to demonstrate how the width of a single Bragg peak behaves as a function of temperature when measured at the S-HRPD beamline. In Fig. 2(a), we plotted the (022) peak of $SrRuO_3$ [22] where the width of the single Bragg peak remains temperature independent over the measured temperature range as expected. The unusual peak broadening seen in the (002)/(220) peak of PFN is naturally explained by a splitting of two reflections, which strengthens on cooling, and would appear to exclude the $R3m$ structure. The origin of this unusual temperature dependence can be found by examining the Fe/Nb-O bond lengths and their temperature dependence, shown in Fig. 2(b). Two aspects are particularly noteworthy: First, there are already four different Fe/Nb-O bond lengths even at room tempera-

ture [see the inset in Fig. 2(b) for the four oxygen atoms with different Fe/Nb–O bond lengths denoted by different numbers]; second, the splitting of the Fe/Nb–O bond lengths only continues to grow upon cooling. Thus, the larger distortion of the (Fe/Nb)O₆ octahedron lies at the heart of the unusual peak broadening seen in Fig. 2(a), favoring the *Cm* space group.

The temperature dependence of the lattice constants and unit-cell volume are summarized in Fig. 3. We also plot the monoclinic angle in pseudocubic notation. Square symbols represent NOVA results, whereas red circles indicate those from S-HRPD. Refinements were performed in the *Pm* $\bar{3}$ *m* structure above T_C and the *Cm* structure below T_C . Both the lattice constants and the unit-cell volume follow a consistent trend without any clear anomaly at the antiferromagnetic transition. Regarding the previous claim of negative thermal expansion [11], we note that there is no evidence of such an effect in the data presented here, taken using either instrument, although it is also important to note that lattice parameters from x-ray diffraction are normally more precise. It is an open question to us why our data collected from two different instruments do not show the negative thermal expansion claimed in Ref. 11.

In order to further analyze the temperature dependence of the unit-cell volume, the Debye-Grüneisen formula [23] was used

$$V(T) = \frac{V_0 U(T)}{Q - bU(T)} + V_0, \quad (1)$$

$$U(T) = 9Nk_B T \left(\frac{T}{\Theta_D} \right)^3 \int_0^{\frac{\Theta_D}{T}} \frac{x^3}{e^x - 1} dx, \quad (2)$$

where $U(T)$ is total internal energy, $Q = V_0 B_0 / \gamma$, $b = (B'_0 - 1) / 2$, γ is the Grüneisen parameter, B_0 and B'_0 are the bulk modulus and its first derivative with pressure, N represents the number of atoms in the unit cell, k_B is the Boltzmann constant, and V_0 is volume at zero temperature. Fitting (shown by a solid line) results in a Debye temperature Θ_D of only 150 K, whereas $b = 1.5$, $V_0 = 64.582 \text{ \AA}^3$, and $Q = 3.87(6) \times 10^{-17} \text{ J}$ are similar to parameters used for other materials [24–26]. We note that the resulting Debye temperature is abnormally small, leading to a bulk modulus around 600 GPa for a typical Grüneisen parameter of order one, which is high for an oxide: For example, we earlier found bulk moduli of 120 GPa for YMnO₃ [27] while 250 GPa has been reported for MgSiO₃ [28]. Note that this assumption about the Grüneisen parameter is crude, and so our estimate of the bulk modulus should be taken with caution. Moreover a true test of the bulk modulus needs to be performed by measuring the volume measurement under pressure. On the other hand, fixing the Debye temperature to the more typical 430 K led to a noticeably poorer fit (dashed line) with $b = 1.5$, $V_0 = 64.595 \text{ \AA}^3$, and $Q = 2.9(1) \times 10^{-17} \text{ J}$. This could be consistent with an

anomaly below T_N but opposite in sign to that reported previously.

Figure 3(d) shows the temperature dependence of atomic displacement parameters u^2 for each atom. The thermal parameter of Pb is much larger than those of O and Fe/Nb, almost comparable to those of other Pb-containing ferroelectric materials [12] and consistent with a previous report [14]. The temperature dependence was modeled using

$$\overline{u^2} = \left(\frac{145.55T}{M\Theta_D^2} \right) \varphi \left(\frac{\Theta_D^i}{T} \right) + A^i \quad (3)$$

$$\varphi \left(\frac{\Theta_D^i}{T} \right) = \frac{T}{\Theta_D^i} \int_0^{\frac{T}{\Theta_D^i}} \frac{x}{e^x - 1} dx, \quad (4)$$

where i represents each atomic species (Pb, Fe/Nb, O), and $A^i = 36.39/M^i\Theta_D^i$ is related to zero-point energy of the atoms concerned with atomic mass M^i [23]. However, it was necessary to add constant offsets to A to achieve better agreement. The final result, denoted by lines in Fig. 3(d), indicated effective Debye temperatures of 150 K for Pb, 680 K for O, and 370 K for Fe/Nb.

Using the structural information, we then searched for possible experimental evidence of magnetoelectric coupling. PFN is known to exhibit a frequency-dependent anomaly in the dielectric constant at T_N , but little else is known of the magnetoelectric coupling. From the high-accuracy structural information presented here, it is possible to calculate the expected ferroelectric polarization, starting from the centrosymmetric *Pm* $\bar{3}$ *m* space group. Using a similar approach, we were previously able to show a negative magnetoelectric coupling in one of the best-studied multiferroic compounds, BiFeO₃ [29]. For simplicity, the nominal valences of the atoms were used as a starting point: Pb²⁺, Fe³⁺, Nb⁵⁺, and O²⁻. Since the actual valences, so-called Born effective charges, which include dynamic terms, might well differ from the nominal charge values [30], the discussion below may not be fully quantitative, but it should be qualitatively correct. Using the above assumptions, the electric polarization was calculated with respect to the paraelectric *Pm* $\bar{3}$ *m* phase. As shown in Fig. 3(e), the estimated polarization at room temperature is around 20 $\mu\text{C}/\text{cm}^2$, which is twice that reported [3, 4] in polycrystalline samples. Considering the rough assumptions made and the fact that the experiments were performed on powder samples, we consider this degree of deviation acceptable. The temperature dependence was then parametrized using Ginzburg-Landau analysis, assuming that the electric polarization follows the usual first-order temperature dependence: $F(P) = \frac{\alpha_2}{2} P^2 + \frac{\alpha_4}{4} P^4 + \frac{\alpha_6}{6} P^6$, where F is the Ginzburg-Landau free energy and P is the polarization. A fit to all points produced an unphysically high Curie temperature, whereas constraining the Curie temperature led to clear systematic trends in the residuals; a fit to only the points above the Néel transition, shown

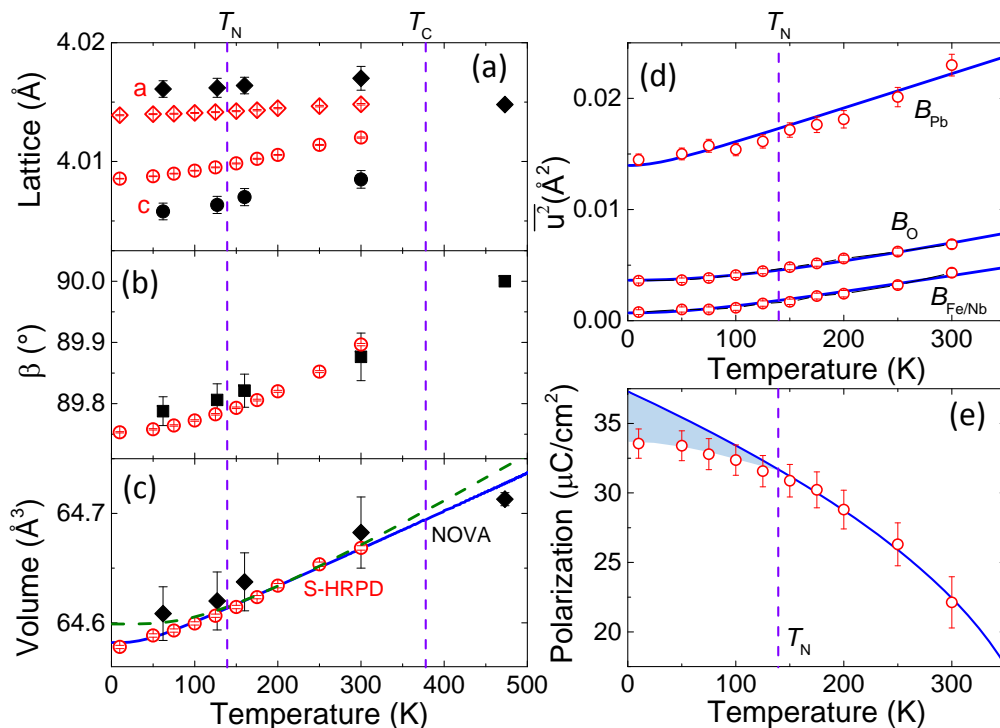


FIG. 3. Temperature dependence of (a) lattice parameters, (b) monoclinic angle, (c) unit-cell volume, (d) thermal parameter, and (e) calculated polarization. The refined unit-cell volume (symbols) is shown together with the theoretical curve obtained from the Debye-Grüneisen formula, and polarization was calculated from the refined atomic positions.

in Fig. 3(e), predicted a Curie temperature of 380 K in close agreement with experiment, but the data appear to deviate from this fit below T_N . This discrepancy, marked by shading in the figure, is the clearest experimental evidence yet of the magnetoelectric coupling in PFN.

For further analysis of the short-range structure, Fig. 4(a) shows how the radial distribution function $G(r)$ calculated from the NOVA data changes gradually with temperature. Of note are the several regions where peaks' intensities increase on cooling. At these short length scales, corresponding to large momentum transfers Q , we can ignore contributions from magnetic scattering because they are usually small compared to nuclear scattering [31]. As shown in Fig. 4(b), the long-range structure up to 100 Å can be well explained by the Cm space group.

First, we consider the short-range structure at high temperatures above the ferroelectric transition. Using the data taken at 453 K, we tested four different models to explain the data and clarify the local structure, all variants of the Cm structure, and all explained in more detail below: (A) one without local short-range structure, (B) one with Pb displacements as considered previously [14], (C) one with Pb disorder, and (D) one with both Pb displacement and O disorder. For all models, Fe and Nb are treated as an average pseudoatom as in the refinement. Models B–D take model A as their starting

point and allow additional freedom in the atomic positions. In departing from model A, C centering was not retained. As shown in Fig. 4(c), the agreement is indeed improved by including Pb displacement and O disorder in our model calculation. Upon closer inspection, model A is found not to satisfactorily explain the intensities of peaks at $r = 2$ and 3.5 Å, and agreement with experimental results is poor at longer distances. It is particularly surprising that, even in the nominally paraelectric phase well above the ferroelectric transition, there is clear evidence of short-range structure. We note that similar behavior is often found in relaxor ferroelectric materials [32, 33]. Thus, our result adds further weight to the previous claim that PFN is a rare relaxor multiferroic.

Having concluded that the simplistic model A does not adequately explain even the high-temperature local structure, we now consider other models which might describe the data at all temperatures. Given lead's large thermal parameter even after accounting for the offset between the Pb and Fe/Nb sublattices in the Cm structure (model A) as shown in Fig. 3(d), it is natural to think of further Pb displacements as an origin of short-range structure as is often the case in closely related Pb-containing perovskite systems [12, 34] and as considered previously [14]. At 62 K, model B requires that the lead atoms shift by $(-0.019, 0.03, 0.012)$ in fractions of the pseudocubic unit cell, less than previously reported [14].

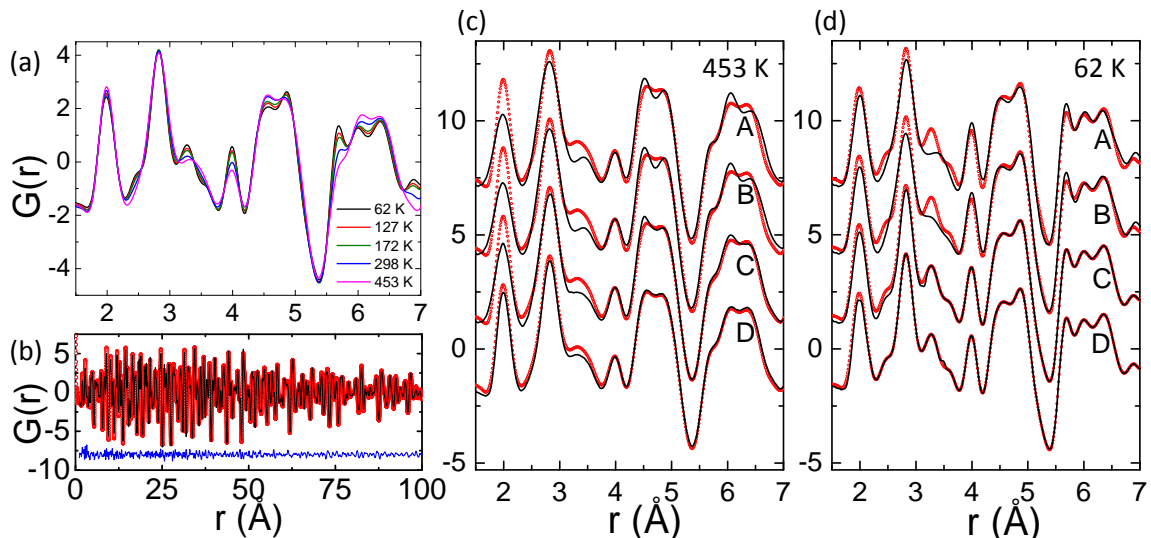


FIG. 4. (a) Radial distribution function $G(r)$ at several temperatures, calculated from NOVA results. Gradual changes may be observed with temperature at several regions of interest (see the text). (b) Radial distribution function $G(r)$ is compared with fitting results over a wide length-scale range for the 62 K data. The symbols represent the data points, whereas the line is the fitting results with the difference curve shown at the bottom. The local structure is compared with several models at (c) 453 K and (d) 62 K. Circles are calculated from experimental data, and lines are fits to several models: Model A assumes no local structure; model B assumes Pb displacements; model C considers Pb disorder; and model D combines Pb displacements with O disorder. Traces have been offset vertically for clarity.

Moving the Pb atoms introduces several peaks between $r = 3$ and 4 \AA , but their intensities are much smaller than in the experimental results, and the peak at $r = 2.5 \text{ \AA}$ is not reproduced. Above the ferroelectric transition, symmetry constrains the Pb displacement to be (η, η, η) , where $\eta = 0.02$ at 453 K. Displacing the Pb atoms in concert, which preserves the unit cell, is quite a simplistic model, and allowing the Pb atoms more freedom of movement should better model the real system. Accordingly, model C was introduced with the possibility of random shifts in the Pb positions.

Model C simulates the effect of Pb disorder using a $4 \times 4 \times 4$ supercell in which each lead atom was allowed to move freely from its original position. Although this model was able to better model the experimental radial distribution function, at least at low temperatures, the average Pb displacement from its already displaced Cm position is 0.2 \AA in this model. This is very large compared to Pb's atomic thermal motion in Fig. 3(d), approaches the upper limit observed in the strongest Pb-based ferroelectrics and BiFeO_3 with one of the highest polarization values of $\sim 86 \mu\text{C}/\text{cm}^2$ [29], and would suggest an electric polarization far exceeding that reported [3, 4]. The comparative success of model C relative to model B is most likely a result of the significantly higher number of free parameters. Although model C is ruled out on the basis of the extremely large displacements compared to the reported polarization values, the fact that it required unphysical displacements of Pb im-

plies that other atoms must also be considered. It has already been shown that the Fe/Nb atoms do not exhibit any significant displacement from their ideal positions [14]. That leaves oxygen, which has a larger thermal parameter and which is well known to depart from its ideal position in most perovskite structures, including in several Pb-containing phases which exhibit oxygen displacement [35–37] or the random rotation of oxygen polyhedra [33]. Model D allows the oxygen atoms to shift.

A further justification for considering O disorder comes from the reported random distribution of neighboring Fe^{3+} and Nb^{5+} [7] and the lack of any features in our data that would suggest even short-range cation order. The magnetic moments calculated from the long-range refinement are $3.4(6) \mu_B$ at 62 K (NOVA) and $3.3(3) \mu_B$ at 10 K (S-HRPD), corresponding to the high spin state of Fe^{3+} , which would make the two cations' sizes essentially identical and eliminate the common source of disorder. The next most probable reason for oxygen atoms to depart from their ideal positions is the displacements of the Pb^{2+} cations from their already-shifted positions, which would be expected to cause small rotations of the $(\text{Fe,Nb})\text{O}_6$ octahedra. This would be frustrated, unless the Pb displacements ordered in one of a few very specific ways which would be expected to produce additional nuclear reflections. An orthogonal possibility arises from the electric-field gradients created by having a random distribution of Fe^{3+} and Nb^{5+} cations. An oxygen atom

situated between an iron and a niobium site feels an electric-field gradient that will polarize it. Meanwhile, Nb^{5+} , having the electronic configuration of krypton, will be unable to share electron density with oxygen, which $3d^5 \text{Fe}^{3+}$ can, using its weakly antibonding e_g^* orbitals. In fact, iron, being a $3d$ transition metal, should have significant on-site electron repulsion and may benefit by donating some of its electron density to its oxygen ligands. All of these electronic effects would produce a net flow of electron density away from iron sites and toward niobium sites with many oxygen atoms caught in the middle. In model D, we combined lead displacement (model B) with oxygen disorder using a $4 \times 4 \times 4$ supercell. Here we allowed oxygen atoms to move freely while all lead atoms were constrained to move together. As one can see in Figs. 4(c) and 4(d), this model apparently fits the experimental results very well. The fitted atomic displacement in fractions of the pseudocubic unit cell for lead is $(0.010, -0.004, 0.008)$ at 453 K, which is reduced compared to model B. For oxygen, the average shifts relative to the original site are (0.0195) at 62 K and (0.0203) at 453 K in fractional coordinates, which is around 0.08 \AA . As is clear in Fig. 4, of the models considered here, model D is the most successful at describing the experimental results, and it does so in a physically reasonable manner.

In Fig. 5, we deconvoluted the contributions of correlations from each pair of atoms using models A and D for the 62 and 453 K data shown in Fig. 4. In each panel, the top six lines show correlation functions between individual pairs of atoms as labeled. Below this are the experimental results and best fit and finally the residuals. A comparison of panels (a) with (b) in Fig. 5 reveals that O-O correlations develop a great deal of additional structure at both temperatures, explaining well the additional peaks at $r = 2.5\text{--}4 \text{ \AA}$.

CONCLUSION

In conclusion, we have undertaken both high-resolution powder-diffraction and total scattering experiments on PFN in order to shed light on the unusual relaxor multiferroicity in this material, focusing on four key aspects of the physical properties: (i) determination of the low-temperature structure, (ii) the experimental examination of the reported negative thermal expansion behavior, (iii) possible structural evidence of magnetoelectric coupling, and (iv) the nature of the relaxor behavior. By combining both long- and short-range diffraction data, it is possible to provide new insight on each of the four issues. First, the high-resolution neutron-diffraction data are more consistent with the Cm space group at low temperatures as reported based on synchrotron data [11] and exclude the previously proposed $R3m$ [7] structure. However, there are no signs of the negative thermal expansion

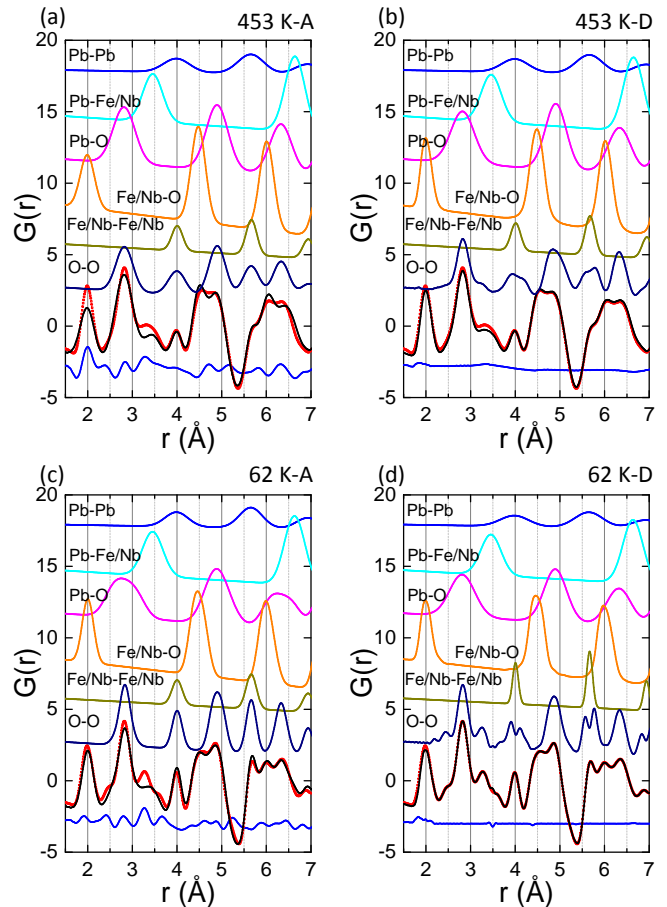


FIG. 5. Atomic position correlations at 453(62) K with (a) [(c)] no local structure and (b) [(d)] both Pb displacement and O disorder. The top six lines show atom-atom radial correlation functions as labeled, followed by the experimental results (circles), best fit (line), and finally its residuals (bottom line). Traces have been offset vertically for clarity.

reported in Ref. 11 with the data instead being well fit by the conventional Debye-Grüneisen formula. We succeeded in finding a structural signature of the magnetoelectric coupling by Ginzburg-Landau analysis of the calculated electric polarization. Finally, the data clearly show that over the entire temperature range covered in this study there exists a short-range structure in addition to the global structure of $Pm\bar{3}m$ or Cm . This local structure occurs through Pb displacement as well as O disorder. That this local structure is present in PFN, even in the paraelectric phase, as seen in relaxor ferroelectric materials may hold the key to the strong frequency dependence seen in the dielectric constant of PFN.

ACKNOWLEDGEMENTS

We thank I.-K. Jeong for useful discussions. This work was supported by IBS-R009-G1. The neutron scattering

experiment was approved by the Neutron Science Proposal Review Committee of J-PARC/MLF (Proposal No. 2012A0017) and supported by the Inter-University Research Program on Neutron Scattering of IMSS, KEK.

* hssim@snu.ac.kr

† jgpark10@snu.ac.kr

- [1] S.-W. Cheong and M. Mostovoy, *Nature Mater.* **6**, 13 (2007).
- [2] M. Fiebig, *J. Phys. D* **38**, R123 (2005).
- [3] A. Kania, E. Talik, and M. Kruczek, *Ferroelectrics* **391**, 114 (2009).
- [4] R. K. Mishra, R. N. P. Choudhary, and A. Banerjee, *J. Phys.: Condens. Matter* **22**, 025901 (2010).
- [5] V. V. Laguta, M. D. Glinchuk, M. Maryško, R. O. Kuzian, S. A. Prosandeev, S. I. Raevskaya, V. G. Smotrakov, V. V. Eremkin, and I. P. Raevski, *Phys. Rev. B* **87**, 064403 (2013).
- [6] J. T. Wang, C. Zhang, Z. X. Shen, and Y. Feng, *Ceramics Int.* **30**, 1627 (2004).
- [7] S. A. Ivanov, R. Tellgren, H. Rundlof, N. W. Thomas, and S. Ananta, *J. Phys.: Condens. Matter* **12**, 2393 (2000).
- [8] E. I. Sitalo, Y. N. Zakharov, A. G. Lutokhin, S. I. Raevskaya, I. P. Raevski, M. S. Panchelyuga, V. V. Titov, L. E. Pustovaya, I. N. Zakharchenko, A. T. Kozakov, and A. A. Pavelko, *Ferroelectrics* **389**, 107 (2009).
- [9] B. Fraygola, N. Frizon, M. H. Lente, A. A. Coelho, D. Garcia, and J. A. Eiras, *Integrated Ferroelectrics: An International Journal* **124**, 53 (2011).
- [10] M. H. Lente, J. D. S. Guerra, G. K. S. de Souza, B. M. Fraygola, C. F. V. Raigoza, D. Garcia, and J. A. Eiras, *Phys. Rev. B* **78**, 054109 (2008).
- [11] S. P. Singh, D. Pandey, S. Yoon, S. Baik, and N. Shin, *Appl. Phys. Lett.* **90**, 242915 (2007), arXiv:0706.0647 [cond-mat.mtrl-sci].
- [12] N. Lampis, P. Sciau, and A. G. Lehmann, *J. Phys.: Condens. Matter* **11**, 3489 (1999).
- [13] A. Mesquita, B. M. Fraygola, V. R. Mastelaro, and J. A. Eiras, *Appl. Phys. Lett.* **100**, 172907 (2012).
- [14] I.-K. Jeong, J. S. Ahn, B. G. Kim, S. Yoon, S. P. Singh, and D. Pandey, *Phys. Rev. B* **83**, 064108 (2011).
- [15] R. Kolesova and M. Kupriyanov, *Phase Transitions* **45**, 271 (1993).
- [16] Y. X. Wang, W. L. Zhong, C. L. Wang, and P. L. Zhang, *Phys. Lett. A* **288**, 45 (2001).
- [17] I.-K. Jeong and S. Park, *J. Korean Phys. Soc.* **59**, 2756 (2011).
- [18] J. Rodríguez-Carvajal, *Physica B* **192**, 55 (1993).
- [19] C. L. Farrow, P. Juhás, J. W. Liu, D. Bryndin, E. S. Bozin, J. Bloch, T. Proken, and S. J. L. Billange, *J. Phys.: Condens. Matter* **19**, 335219 (2007).
- [20] Multiplying by the matrix $\begin{pmatrix} 1/\sqrt{2} & 1/\sqrt{2} & 0 \\ -1/\sqrt{2} & 1/\sqrt{2} & 0 \\ 0 & 0 & 1 \end{pmatrix}$ converts the monoclinic structure to the pseudocubic structure.
- [21] R. Kolesova, V. Kolesov, M. Kupriyanov, and R. Skulski, *Phase Transitions* **68**, 621 (1999).
- [22] S. Lee, J. R. Zhang, S. Torii, S. Choi, D.-Y. Cho, T. Kamiyama, J. Yu, K. A. McEwen, and J.-G. Park, *J. Phys.: Condens. Matter* **25**, 465601 (2013), arXiv:1310.1686 [cond-mat.str-el].
- [23] I. G. Wood, K. S. Knight, G. D. Price, and J. A. Stuart, *J. Appl. Cryst.* **35**, 291 (2002).
- [24] A. Y. Wu and R. J. Sladek, *Phys. Rev. B* **27**, 2089 (1983).
- [25] S. Lee, J.-G. Park, D. T. Adroja, D. Khomskii, S. Strelsov, K. A. McEwen, H. Sakai, K. Yoshimura, V. I. Anisimov, D. Mori, R. Kanno, and R. Ibberson, *Nature Mater.* **5**, 471 (2006).
- [26] J. Park, S. Lee, M. Kang, K.-H. Jang, C. Lee, S. V. Streltsov, V. V. M. M. V. Valentyuk, J. E. Medvedeva, T. Kamiyama, and J.-G. Park, *Phys. Rev. B* **82** (2010), 10.1103/PhysRevB.82.054428.
- [27] D. P. Kozlenko, S. E. Kichanov, S. Lee, J.-G. Park, V. P. Glazkov, and B. N. Savenko, *JETP Lett.* **82**, 193 (2005).
- [28] D. Andrault, N. Bolfan-Casanova, and N. Guignot, *Earth Planet. Sci. Lett.* **193**, 501 (2001).
- [29] S. Lee, M. T. Fernandez-Diaz, H. Kimura, Y. Noda, D. T. Adroja, S. Lee, J. Park, V. Kiryukhin, S.-W. Cheong, M. Mostovoy, and J.-G. Park, *Phys. Rev. B* **88**, 060103(R) (2013), arXiv:1307.1519 [cond-mat.str-el].
- [30] R. D. King-Smith and D. Vanderbilt, *Phys. Rev. B* **47**, 1651(R) (1993).
- [31] T. Egami and S. J. L. Billinge, *Underneath The Bragg Peaks: Structural Analysis of Complex Materials* (Pergamon, 2003) Chap. Magnetic Correlation Functions.
- [32] I.-K. Jeong, T. W. Darling, J. K. Lee, T. Proffen, R. H. Heffner, J. S. Park, K. S. Hong, W. Dmowski, and T. Egami, *Phys. Rev. Lett.* **94**, 147602 (2005), arXiv:cond-mat/0412173.
- [33] T. Egami, E. Mamontov, W. Dmowski, and S. B. Vakhrushev, *AIP Conf. Proc.* **677**, 48 (2003).
- [34] C. Malibert, B. Dkhil, J. M. Kiat, D. Durand, J. F. Bérar, and A. S. de Biré, *J. Phys.: Condens. Matter* **9**, 7485 (1997).
- [35] W. Dmowski, M. K. Akbas, P. K. Davies, and T. Egami, *J. Phys. Chem. Solids* **61**, 229 (2000).
- [36] G. Baldinozzi, P. Sciau, and J. Lapasset, *Phys. Status Solidi A* **133**, 17 (1992).
- [37] I. W. Chen, *J. Phys. Chem. Solids* **61**, 197 (2000).